Engineering Fracture Mechanics 208 (2019) 189–208

Contents lists available at ScienceDirect

Engineering Fracture Mechanics

journal homepage: www.elsevier.com/locate/engfracmech

Effects of moisture gradient of concrete on fracture process in restrained concrete rings: Experimental and numerical

Wei Dong[a], Xiaoyu Zhao[a], Xiangming Zhou[b,*], Wenyan Yuan[a]

[a] State Key Laboratory of Coastal and Offshore Engineering, Dalian University of Technology, Dalian 116024, PR China
[b] Civil Engineering Design, Department of Civil and Environmental Engineering, Brunel University London, UB8 3PH, United Kingdom

ARTICLE INFO

Keywords:
Concrete cracking
Crack propagation
Elliptical ring test
Moisture gradient
Shrinkage cracking

ABSTRACT

The non-uniform shrinkage caused by moisture gradient in concrete provides self-restraint, which has a significant effect on the assessment of cracking potential of concrete through the restrained shrinkage ring test. Furthermore, moisture gradient in concrete would be also affected by concrete strength because concretes designed for different strength grades usually have different water to cement ratio. In this paper, three series of circular and elliptical concrete rings with a 37.5 mm thick wall and three distinguished concrete strength grades of C30, C50 and C80 were tested to investigate the effect of the moisture gradient on crack initiation and propagation in restrained concrete rings. An integrative model based on the nonlinear diffusion theory is introduced to calculate the moisture distributions in concrete rings, and the fictitious temperature fields are derived for the simulation of the shrinkage effect in concrete. Meanwhile, a fracture mechanics-based numerical method is proposed to analyze the crack initiation and propagation in a concrete ring in the restrained ring test. The effects of ring geometry, concrete strength and uniform/non-uniform shrinkage assumption on the cracking initiation and propagation process are elaborated. The results indicate that the non-uniform shrinkage in concrete provides driving energy for concrete cracking, which is approximately 40% of the total driving energy. Accordingly, it significantly affects the crack initiation position and propagation direction, occurring at the outer surface and propagating toward the inner surface of the concrete ring. With the increase of concrete strength, the cracking potential of restrained concrete ring increases and the proportion of the self-restraint caused by the non-uniform shrinkage in the total restraint decreases because of the reduced moisture distribution.

1. Introduction

The durability of many concrete structures with a large and exposed surface area-to-volume (A/V) ratio such as paving/floor slabs, bridge decks etc. are often threatened by shrinkage cracking at early ages. Cracks in concrete structures provide a transmission path for water and other chemical agents to intrude inside, leading to the corrosion of reinforcing steel and deterioration of the concrete [1]. Faced with the risk of early-age shrinkage cracking, many efforts have been made to reduce the cracking sensitivity of concrete including the application of fibre reinforcement [2], the addition of shrinkage reducing admixtures [3] and internal curing [4]. Simultaneously, several test methods have been developed to assess the cracking sensitivity of concrete and other cement-based

* Corresponding author.
E-mail addresses: dongwei@dlut.edu.cn (W. Dong), Zhaoxiaoyu_lv@mail.dlut.edu.cn (X. Zhao), xiangming.zhou@brunel.ac.uk (X. Zhou), yuanwenyan@mail.dlut.edu.cn (W. Yuan).

https://doi.org/10.1016/j.engfracmech.2019.01.011
Received 18 July 2018; Received in revised form 29 October 2018; Accepted 7 January 2019
Available online 14 January 2019
0013-7944/

Nomenclature

a, b	fitted coefficients of mechanics and fracture properties of concrete
A, B, P, n	parameters for calculating cement hydration rate
D	moisture diffusion coefficient
E	elastic modulus of concrete
f_t	splitting tensile strength of concrete
G_f	fracture energy of concrete
H	interior moisture in early-age concrete
H_c	interior moisture caused by cement hydration
H_d	interior moisture caused by moisture diffusion
i	crack propagation step
K_{IC}^{ini}	initial fracture toughness
K_I^S	stress intensity factor caused by concrete shrinkage
$K_{I\,steel}^S$	stress intensity factor caused by external restraint from the central steel ring
$K_{I\,self}^S$	stress intensity factor caused by self-restraint from the non-uniform shrinkage
K_I^σ	stress intensity factor caused by the cohesive stress
R_0	inner radius of a circular concrete ring
R_1	major inner radius of an elliptical concrete ring
R_2	minor inner radius of an elliptical concrete ring
t	age of concrete
w	crack opening displacement
w_0	stress-free crack opening displacement
w_s	displacement corresponding to the break point in the bilinear σ-w relationship
α	degree of hydration
α_c, α_u, H_{cu}	parameters for calculating the interior moisture caused by cement hydration H_c
σ	softening stress
σ_s	stress corresponding to the break point in the bilinear σ-w relationship

materials under restrained shrinkage [5]. Due to its simplicity and versatility, the restrained ring test has been widely adopted by researchers for assessing the cracking potential of concrete and other cement-based materials for several decades [6]. This has led to the investigation of its parameters on the fracture mechanism of concrete, including the effects of ring geometry, both circular [7,8] and elliptical [9,10], and drying directions from the top and bottom surfaces [11,12] and outer circumference [13,14].

To standardize the restrained ring test, the American Association of State Highway and Transportation Officials (i.e. AASHTO PP34-99: Standard Practice for Cracking Tendency using a Ring Specimen) and American Society for Testing and Materials (i.e. the ASTM C1581/C1581M-09a: Standard Test Method for Determining Age at Cracking and Induced Tensile Stress Characteristics of Mortar and Concrete under Restrained Shrinkage) recommended a thick (75 mm) and a thin (37.5 mm) concrete ring, respectively, as the normative sizes of concrete rings. Both organizations suggested the drying of the concrete rings from the outer circumference by sealing top and bottom surfaces. During drying, the moisture near the drying surface evaporates into the environment quicker, with the interior moisture moving toward the drying surface along the radial direction. Due to differential drying, the region near the drying surface shrinks faster than the inner area, causing higher tensile stress to develop at the surface even if the restraint from the inner steel ring is not there [14–16]. Therefore, the non-uniform shrinkage caused by the moisture gradient provides the self-restraint to drive concrete cracking, together with the external restraint provided by the inner steel ring. In the case of a thick concrete ring, it has been proven that the self-restraint plays a leading role in driving the concrete crack to initiate and propagate [14,17]. To reduce the self-restraint effect, drying from the top and bottom surfaces were employed by many researchers in the restrained ring tests [12,13,18–20]. Furthermore, in the case of a thin concrete ring, the moisture gradient and thus non-uniform shrinkage become insignificant due to the relatively short moisture diffusion distance. On this account, some researchers [21–27] assumed that the moisture reduction caused by the moisture diffusion was coincident along the radial direction, and the induced shrinkage strain was uniform within the whole cross-section of a concrete ring. Based on the uniform shrinkage assumption, the analytical method was used to analyze the stress distribution in the concrete rings [7,18] and the formation process of shrinkage cracks. The results indicated that, upon the uniform shrinkage assumption, the cracks in a restrained concrete ring would initiate at inner surface of a concrete ring and propagate towards its outer surface) [11,27].

It should be noted that, under the uniform shrinkage assumption, the self-restraint caused by non-uniform shrinkage is completely neglected, resulting in the external restraint provided by a steel ring being overrated. In fact, according to the diffusion theory [28,29], the moisture distribution within early-age concrete is highly nonlinear especially near the drying surface even for a thin concrete element. It is not certain whether the moisture gradient induced non-uniform shrinkage influences shrinkage cracking formation as well as how the fracture mechanism in the ring test works with respect to concrete having different moisture gradients. In addition, the elliptical geometry has been verified to be effective for accelerating the shrinkage cracking in a 37.5 mm-thick concrete ring, i.e. a thin ring. Due to its particular geometry, stress concentration exists at the inner surface of major radius and the degree of restraint to a specimen increases significantly compared with the traditional circular geometries recommended by ASTM [10,27]. However, these characteristics of an elliptical ring were analyzed under the uniform shrinkage assumption [10,27]. When the non-uniform shrinkage along the radial direction was taken into consideration, the induced self-restraint results in much higher tensile stress near the outer surface of a concrete ring, weakening the restraint effect provided by the elliptical geometry. It is not clear whether the restrained elliptical ring has the aforementioned advantage under the combined effects of external restraint and self-restraint. Thus, it is significant to investigate the composition of restraint effects for various moisture gradients to comprehensively assess the cracking resistance of concrete using the ring test.

To investigate the effect of the moisture gradient on the early-age cracking potential of concrete requires an accurate assessment of the moisture distribution when considering non-uniform shrinkage along the radial direction. There exist two types of approaches, i.e. experiment-based approach and analysis-based approach, which have been commonly utilized to determine the moisture distribution within the concrete. In the experiment-based approach, humidity sensors are placed at different drying depths to measure

the relative humidity, and obtain the moisture distribution by curve fitting the experimental data [30,31]. The derived data in the test can objectively reflect the moisture field, and the fitted expression of moisture distribution is also easily used in the numerical simulation. However, it is impossible to extend the fitted expression to concrete of different mixtures. In the analysis-based approach, the diffusion theory [28,29] based on the second Fick's law is introduced to calculate the moisture diffusion process within the concrete. Using the linear diffusion approach, Moon and co-workers [14] calculated the moisture distribution caused by water diffusion along the radial direction of a concrete ring. It has been proven that the moisture diffusion coefficient is highly nonlinear with respect to relative humidity [32]. The linear diffusion approach may be reasonable only for the short-term drying condition. In addition, the moisture reduction caused by cement hydration, which affects the moisture diffusion process, has not been considered in the published literature [33]. Recently, Zhang et al. [34,35] proposed an integrative model to calculate the moisture distribution within the concrete, in which interaction between cement hydration and moisture diffusion was taken into account, allowing for the moisture diffusion coefficient to be derived based on the nonlinear diffusion equation. The model has been validated by comparison of experimental and theoretical results, hence why it was adopted to calculate the moisture distribution in a concrete ring in this study.

The moisture distribution, which affects the crack formation process and the composition of restraint effects in a restrained shrinkage concrete ring, is simultaneously affected by the water-to-cement (W/C) ratio of concrete. In general, for concrete with a low W/C ratio, the cement hydration and consequent self-desiccation are strong, resulting in a higher tensile strength and elastic modulus, free shrinkage and reduced moisture distribution [36]. Meanwhile, the influence of the W/C ratio on the fracture mechanism of the restrained concrete ring is complex. On the one hand, for a concrete with a low W/C ratio, the high tensile strength increases the concrete's capacity to resist the tensile stress, while large free shrinkage increases the cracking potential of restrained shrinkage concrete ring. On the other hand, a large elastic modulus reduces the degree of restraint of the restrained concrete ring [8], while the slight moisture gradient increases the ratio of a steel ring's restraint to the total restraint effects in the crack formation process. For a qualitative assessment of the cracking potential of different strength grade concretes, the proposal of an effective fracture mechanics-based method is required to investigate the fracture mechanism of restrained concrete rings with different W/C ratios.

In summary, both the self-restraint caused by the non-uniform shrinkage of concrete and the external restraint from the inner steel ring contribute to the driving force, enabling crack initiation and subsequent propagation in the restrained concrete ring. The uniform shrinkage assumption is not appropriate for thin rings with a 37.5 mm-thick concrete ring wall because, under this assumption, crack initiation would be solely caused by external restraint (i.e. from the central restraining steel ring). Meanwhile, the moisture distribution equation, fitted from experimental data from only normal strength concrete, does not necessarily apply to other grades of concrete. In addition, the moisture distribution equation cannot explicitly take into account the effects of some significant parameters such as the W/C ratio, cement hydration, moisture diffusion etc. In line with this, the objective of this paper is to investigate the fracture mechanism of restrained concrete rings of different strength grades, reveal the influence of the moisture gradient induced non-uniform shrinkage and clarify the composition of restraint effects in the crack formation process. A numerical approach was developed to analyze the crack initiation and propagation process of the restrained shrinkage concrete rings with respect to two geometries (circular and elliptical) and three distinguished concrete strength grades (C30, C50 and C80). Firstly, the moisture distribution in a concrete ring was determined by the integrative model proposed by Zhang et al. [33–35]. A fictitious temperature field, which corresponds to the moisture field, was derived to simulate the mechanical effect of shrinkage of concrete. Furthermore, by introducing the fictitious crack model [37] and the crack propagation criterion [38,39], the crack initiation and propagation process of restrained concrete rings were simulated, and the composition of the restraint effects in the crack formation process with respect to concrete strength was discussed.

2. Experimental programs and results

The concrete of three distinguished strength grades, i.e. C30, C50 and C80, was tested in this study. The same materials and mix proportions of concrete investigated by Zhang et al. [35,36] were used in the tests so that the moisture distributions could be calculated based on the same parameters. The concrete mixtures were made with Grade R42.5 Portland cement. Natural sand and crushed limestone with a maximum particle size of 5 mm and 15 mm were used as fine and coarse aggregates, respectively. The concrete mixture proportions of three strength grades are listed in Table 1. The uniaxial compressive strengths for the C30, C50 and C80 concrete are 32.5 MPa, 49.3 MPa and 86.1 MPa, respectively.

The basic mechanical properties, fracture properties, free shrinkage and restrained circular/elliptical ring tests were conducted in this study on C30, C50 and C80 grade concrete. After curing in the sealed moulds for 24 h, all the specimens were demoulded and moved into an environmental chamber maintained at 23°C and 50% relative humidity (RH) for continued curing until the designated

Table 1
Mixture proportions of concretes with three strength grades (kg/m^3).

Concrete	W/C	Cement	Water	Sand	Stone	Silica fume	Fly ash
C30	0.62	240	186	750	1150	–	60
C50	0.43	345	185	685	1090	–	85
C80	0.30	450	150	580	1140	50	–

age of testing.

2.1. Mechanics and fracture properties

Mechanical and fracture properties of the concretes, including elastic modulus E, splitting tensile strength f_t, fracture energy G_f, and initial fracture toughness K_{IC}^{ini}, were measured at 3, 7, 14, 21, 28 days, respectively. The methods recommended in [40] and [41] were used in this study to calculated fracture energy G_f, and initial fracture toughness K_{IC}^{ini}, respectively. Experiment data were then fitted to a continuous curve by a specified function of Eq. (1).

$$y = a + b \times \ln(t) \tag{1}$$

where t is the age (unit: day) of concrete, and a and b are the fitted coefficients. By substituting the parameters a and b listed in Table 2 into the expression, the mechanical and fracture properties of the concretes of the three distinguished strength grades from 1 to 28 days can be obtained. The experimental data and fitted curves are illustrated in Fig. 1.

2.2. Restrained circular/elliptical ring tests

The restrained circular/elliptical concrete ring tests were conducted to measure the shrinkage cracking of C30, C50 and C80 grade concrete. Two specimens were prepared for every configuration and a total of 12 specimens were tested in this study. The geometries of the circular and elliptical ring specimens are shown in Fig. 2. The inner radius of the circular concrete ring is denoted as R_0, and the major and minor inner radii of the elliptical concrete ring are denoted as R_1 and R_2, respectively. For the ring specimens tested in this study, R_0 and R_1 were chosen as 150 mm, and R_2 was chosen as 75 mm (i.e. $R_0 = R_1 = 2R_2 = 150$ mm, $R_1/R_2 = 2$). The elliptical ring with a ratio of major to minor radius between 2 and 3 has been proven to be more effective to enable a concrete ring crack earlier [26]. The specimen height was 75 mm, and the thicknesses of the concrete and steel rings were set as 37.5 mm and 12.5 mm, respectively, which are recommended by ASTM.

After demolding, the circular and elliptical concrete rings were sealed with a double-layer aluminium tape on their top and bottom surfaces immediately to allow drying from their outer circumferences only. Four strain gauges were attached on the inner surface of the steel ring to record its strains, as shown in Fig. 3(a). Then, the ring specimens were moved into a standard curing chamber with 23℃ and 50% relative humidity (RH), as shown in Fig. 3(b). The ages corresponding to the first crack occurrence in concrete (see Table 3) can be determined by the sudden drops of the recorded strains of the steel ring. Because the measured strains of steel rings show the similar tendency for the C30, C50 and C80 concrete ring specimens, only the strain curves of the steel ring for C30 ring specimens, as examples, is presented in Fig. 4.

It can be seen from Table 3 that strength grade has a significant effect on the cracking age of a restrained shrinkage concrete ring. For both circular and elliptical geometries, the C30 concrete rings cracked 5–6 days after the C50 concrete rings and 8–10 days after the C80 concrete ones. This indicates that, with the increase of concrete strength, the restrained concrete ring is more sensitive to the restrained shrinkage cracking, which is coincident with Ref. [42]. In addition, the ring geometry also has significant effects on the cracking age as well as cracking positions of a restrained concrete ring [17]. The elliptical rings cracked earlier than the circular ones for all C30, C50 and C80 concrete, which proved that the elliptical geometry could enable the concrete ring to crack earlier for normal strength, middle strength and high strength concretes. Also, the shrinkage cracks would occur near the major radius of an elliptical ring rather than randomly along the circumference of a circular ring, as shown in Fig. 5.

2.3. Free shrinkage

To reflect the shrinkage characteristics of the concrete used in this study, free shrinkage prismatic specimens with the same sectional dimensions and drying conditions as the ring specimens were tested. The cross-section of the prism specimens was the same as the ring specimen, i.e. 75 mm × 37.5 mm, and the length of prism specimen was chosen as 300 mm according to the standard (ISO 1920-8, Testing of concrete - Part 8: Determination of Drying Shrinkage of Concrete for Samples Prepared in the Field or in the Laboratory. 2009). Only a 300 mm × 75 mm surface exposed to the environment for drying while all other surfaces were sealed using a double-layer aluminium tape. The magnitudes of free shrinkage were measured by mechanical dial gauges (see Fig. 6(a)) with the deformations being recorded twice a day. By fitting the measured data, free shrinkage strains of the C30, C50 and C80 concrete at any age between 0 and 28 days can be derived, as shown in Fig. 6(b).

Table 2
Values for the fitted coefficients of a and b.

Concrete grade	E (GPa)		f_t (MPa)		G_f (N/m)		K_{IC}^{ini}(Mpa·m$^{1/2}$)	
	a	b	a	b	a	b	a	b
C30	10.017	5.161	0.487	0.314	39.219	12.622	0.195	0.084
C50	16.050	4.622	0.933	0.540	48.651	16.309	0.200	0.142
C80	24.383	4.242	1.360	0.818	50.381	20.881	0.300	0.149

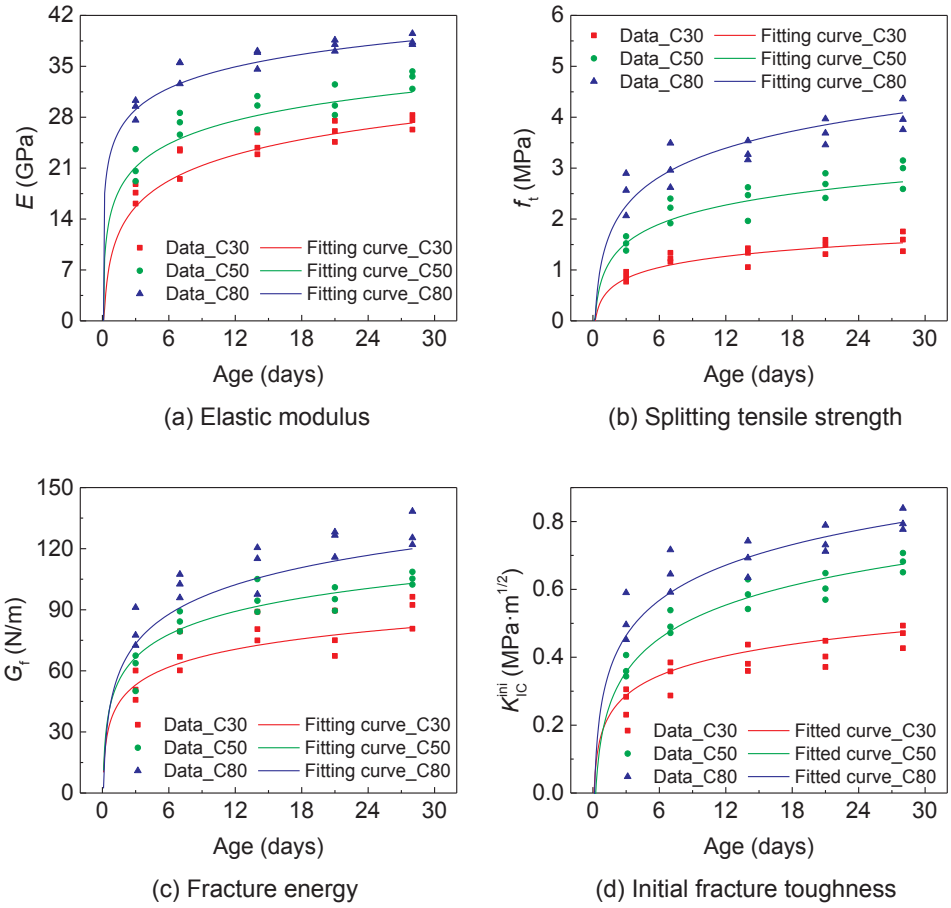

Fig. 1. Experimental data and fitted curves of mechanics and fracture properties.

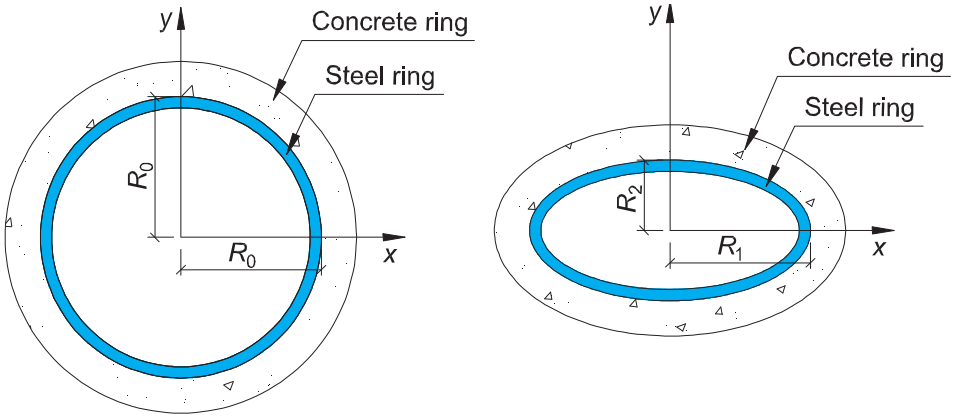

Fig. 2. Geometries of the restrained circular and elliptical rings.

3. Numerical simulations

The numerical simulations were carried out using ANSYS FE code to investigate the fracture mechanism of the restrained shrinkage ring tests on the concrete rings with three distinguished strength grades. Because the ANSYS code does not directly support shrinkage loading neither does it allow a direct entry for shrinkage as a material property, the shrinkage of concrete is assumed to be caused by a fictitious temperature drop applied to it which causes the same value of strain as that induced by shrinkage. According to Zhang et al. [43], the interior humidity can serve as the driving force for both autogenous shrinkage and drying shrinkage of concrete. Thus, a fictitious temperature field was derived for concrete rings based on moisture distribution and free shrinkage strain of

Fig. 3. Instrumented concrete ring and standard curing chamber.

Table 3
Average cracking ages (in days) of grade C30, C50 and C80 concrete rings.

Ring type	Concrete strength grade		
	C30	C50	C80
Circular	21	16	11
Elliptical	17	11	9

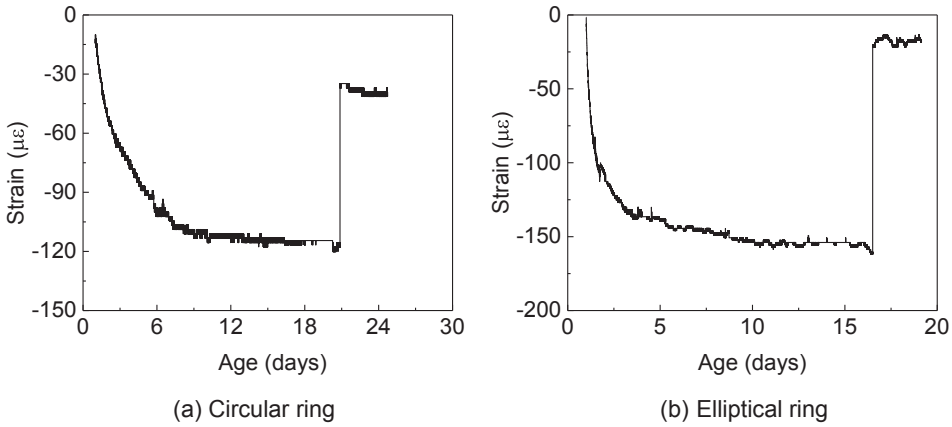

Fig. 4. Strain curves of steel rings for C30 concrete ring specimens.

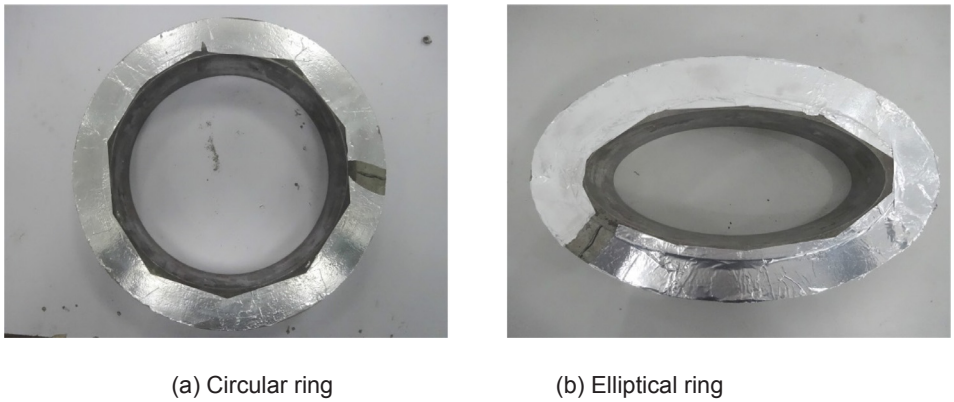

Fig. 5. Shrinkage crack position of restrained circular and elliptical concrete rings.

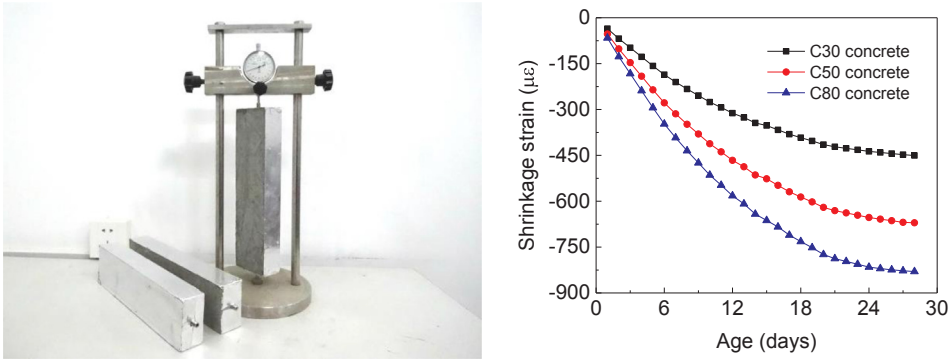

(a) Set-up of free shrinkage test (b) Free shrinkage strains

Fig. 6. Free shrinkage test set-up and results.

concrete. In the numerical analyses, the derived fictitious temperature field was applied to the concrete rings to simulate the mechanical effect of shrinkage of concrete. As for the behaviour of the restrained concrete ring, this can be obtained by a combined thermal and structural analysis. By introducing the fictitious crack model [37], a fracture mechanics-based method was utilized to investigate the complete crack initiation and propagation of concrete in the restrained shrinkage ring tests. Considering the viscoelasticity of concrete, the elastic modulus of concrete at early ages (from 1 to 28 days) was reduced to 60% to take into account the creep effect of concrete in the structural analysis [8,12,44].

3.1. Derivations of moisture distribution and fictitious temperature field

To consider the effect of the moisture gradient on the fracture process in the restrained shrinkage ring test, it is significant to obtain an accurate moisture distribution in concrete. In this study, an integrative model proposed by Zhang et al. [33–35] was introduced to calculate the moisture distribution in the concrete rings with three distinguished strength grades under drying from the outer circumferential surface. The model was briefly described as follows.

The interior moisture (H) in early-age concrete is consumed by cement hydration (H_c) and moisture diffusion (H_d) synchronously so that the cement hydration and moisture diffusion can be regarded as occurring successively during a short duration dt. In each time step dt, the cement hydration occurs primarily and results in the moisture reduction ΔH_c. Accordingly, the remaining moisture $H - \Delta H_c$ (denoted as H_d here) is regarded as the initial humidity to analyze the moisture diffusion process during the same time increment dt. After the moisture diffusion analysis, the result is the relative humidity taking both cement hydration and moisture diffusion into account during the time duration dt. For the restrained shrinkage concrete ring under outer circumference drying, the movement of interior moisture is only along the radial direction. According to Fick's second law of diffusion, the balance of relative humidity in one-dimensional moisture diffusion (x) can be established in Eq. (2).

$$\frac{\partial(H_d)}{\partial t} = \frac{\partial}{\partial x}\left(D\frac{\partial(H_d)}{\partial x}\right) \tag{2}$$

where D is the moisture diffusion coefficient depending on the pore humidity and the mix proportion of concrete.

To derive the moisture distribution, it is necessary to determine the parameters ΔH_c and D. According to Zhang et al. [33–35], the hydration degree-based model [45] was employed to calculate the moisture reduction (ΔH_c) caused by cement hydration. In this model, the degree of hydration (α) and the corresponding relative humidity (H_c) were measured by conducting an adiabatic test of concrete, allowing for the relationship between α and H_c to be obtained from Eq. (3). Under drying conditions, the effect of relative humidity on cement hydration should be considered, so that the relationship between relative humidity and the rate of hydration reaction can be formulated by Eq. (4).

$$H_c = \begin{cases} 1 \text{ for } \alpha \leqslant \alpha_c \\ (1 - H_{c,u})\left(\frac{\alpha - \alpha_c}{\alpha_u - \alpha_c}\right)^{\beta} \text{ for } \alpha > \alpha_c \end{cases} \tag{3}$$

$$\frac{d\alpha}{dt} = \left(\alpha_c \cdot \frac{B}{A}\left(\ln\left(\frac{\alpha_u}{\alpha}\right)\right)^{\frac{B+1}{B}} - P\right)(RH)^n + P \tag{4}$$

The cement hydration degrees α_t and α_{t+dt} at times t and t + dt can be calculated by integrating Eq. (3) from 0 to t and t + dt, respectively. Then, the moisture reduction caused by cement hydration (ΔH_c) during dt can be calculated using Eq. (3). In addition, the humidity-dependent moisture diffusion coefficient D can be determined based on the combination of experimental measurement and nonlinear diffusion analysis [32]. To match the parameters from the experiment, concrete with the same mixture proportions as those investigated by Zhang et al. [35,36] were prepared and tested in this study. The humidity dependent moisture diffusion

coefficients (D) for concretes used in this study are presented in Fig. 7. The diagram to calculate the moisture distribution is shown in Fig. 8, and the calculation process is described as follows.

1. At the beginning drying age t_0, initial degree of hydration $\alpha_0 = \alpha_c$, initial moisture $RH_0 = 100\%$ for Points 1, 2, 3, 4…m.
2. During a time increment from t_0 to t_1, the hydration reaction ratio $d\alpha/dt$ based on RH_0 can be calculated using Eq. (4), and the hydration degree α_1 can be derived by integrating $d\alpha/dt$ from t_0 to t_1. Thereafter, the moisture reduction caused by cement hydration ΔH_c can be determined using Eq. (3).
3. Calculate the moisture diffusion coefficient D_0 based on the RH_0 according to Fig. 7. Let $H_d = RH_0 - \Delta H_c$ as the initial moisture to analyze the moisture diffusion from t_0 to t_1. The moisture RH_1 for Points 5, 6, 7, 8…n can be determined by solving Eq. (2).
4. Repeat steps 1–3 for times t_1, t_2 until the 28 days.

Based on the integrative model, the moisture distribution in the concrete rings with three strength grades can be determined by a step-by-step integration process with respect to time, with the results presented in Fig. 9. More details for the humidity calculation and the model verification can be found in the work by Zhang et al. [33–35].

According to Moon et al. [14], the relationship between moisture distribution and shrinkage strain has been verified as being linear in the case of high relative humidity, i.e. RH > 50%. Thus, a fictitious temperature field, proportional to the moisture distribution, was applied to the prismatic specimens to calculate the shrinkage strain. By comparing with the shrinkage strains measured in the free shrinkage tests, the fictitious temperature field can be determined which is then applied to the concrete rings. The derived fictitious temperature fields applied in the numerical model at 1, 3, 7, 14, 21, 28 days for the three grades of concrete are illustrated in Fig. 10. The fictitious temperature fields at other ages can be determined through linear interpolation.

3.2. Simulation on crack initiation and propagation in a concrete ring

Numerical analyses were conducted on the restrained shrinkage concrete rings with two geometries, i.e. circular and elliptical, and three strength grades, i.e. C30, C50 and C80. Firstly, a thermal analysis was carried out to calculate the fictitious temperature distribution in concrete rings under the derived fictitious temperature field presented in Fig. 10. Taking the circular and elliptical rings of grade C30 concrete as examples, the fictitious temperature distributions of circular and elliptical rings at 14 days are shown in Fig. 11(a) and (b), respectively.

After that, a fracture mechanics-based structural analysis was conducted to investigate the crack initiation and propagation in a concrete ring under restrained shrinkage. Because the shrinkage of a concrete ring under drying is restrained by the inner steel ring, tensile stress will occur in concrete. Therefore, a structural analysis was firstly carried out to calculate the tensile stress distribution in a circular/elliptical concrete ring, and then an initial crack was set in the numerical model of the restrained ring test. In the research of Ouyang and Shah [46], the initial crack length was chosen as 2 mm for concrete elements in fracture analysis. Their study indicated that, as long as this value remains reasonably small, the overall fracture analysis results on the same concrete elements but with different initial crack lengths were very close. Therefore, to reduce the effects of the arbitrariness of a_0 on fracture analysis results of an actually un-cracked concrete ring specimen, a_0 should be as reasonably small as possible, which was chosen as 2 mm in this study for both the circular and the elliptical concrete rings. For the elliptical ring, the initial crack was set where the maximum tensile stress occurs. However, for the circular ring, the maximum tensile stress is the same on the outer circumferential surface of the circular ring. Therefore, in this case, the initial crack was set randomly at the outer circumferential surface of the concrete ring. Meanwhile, to eliminate the effect of the initial crack on analytical results, the cohesive stress acts along the initial crack length in the following numerical simulation step of crack propagation. According to the fictitious crack model proposed by Hillerborg et al. [38], there exists a fracture process zone (FPZ) ahead of the microcracks, which characterises the strain softening and localisation behaviour through the relationship of the cohesive stress (σ) with the crack opening displacement (w). In this study, a bilinear tension-softening relationship between σ and w was introduced to describe the nonlinear characteristics of concrete in FPZ, which is illustrated in

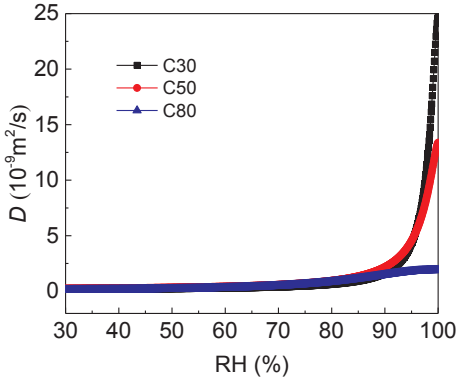

Fig. 7. Variations of humidity dependent moisture diffusion coefficient D.

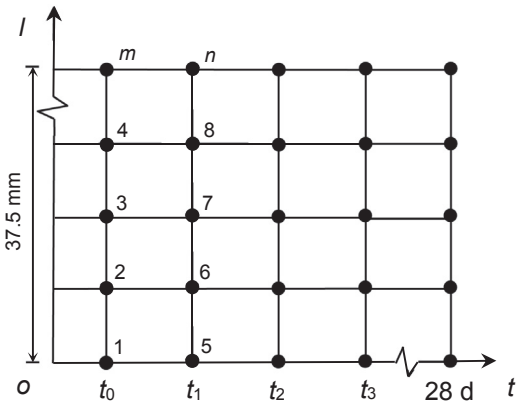

Fig. 8. Diagram to calculate the moisture distribution.

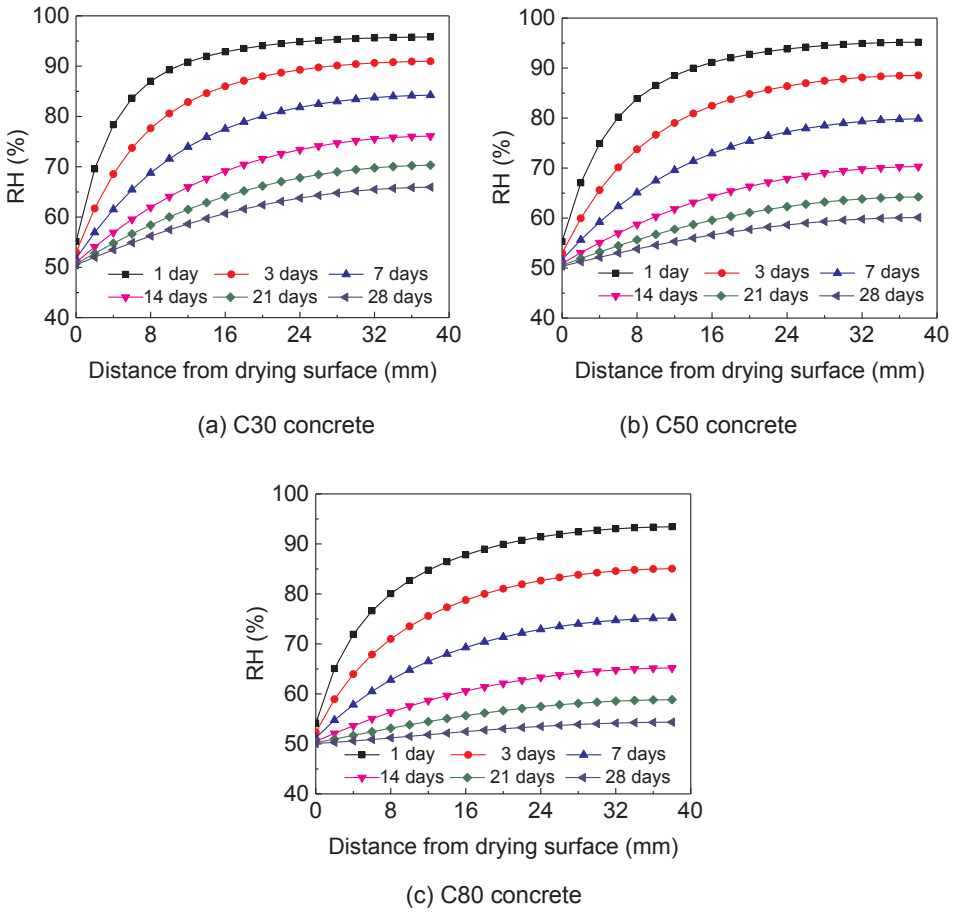

Fig. 9. Moisture distributions in restrained concrete rings.

Fig. 12.

According to Peterson's research [47], σ_s, w_s and w_0 can be determined as follows:

$$\sigma_s = f_t/3 \tag{5}$$

$$w_s = 0.8G_f/f_t \tag{6}$$

$$w_0 = 3.6G_f/f_t \tag{7}$$

where w_0 is the stress-free crack opening displacement, and w_s and σ_s are the displacement and the stress corresponding to the break

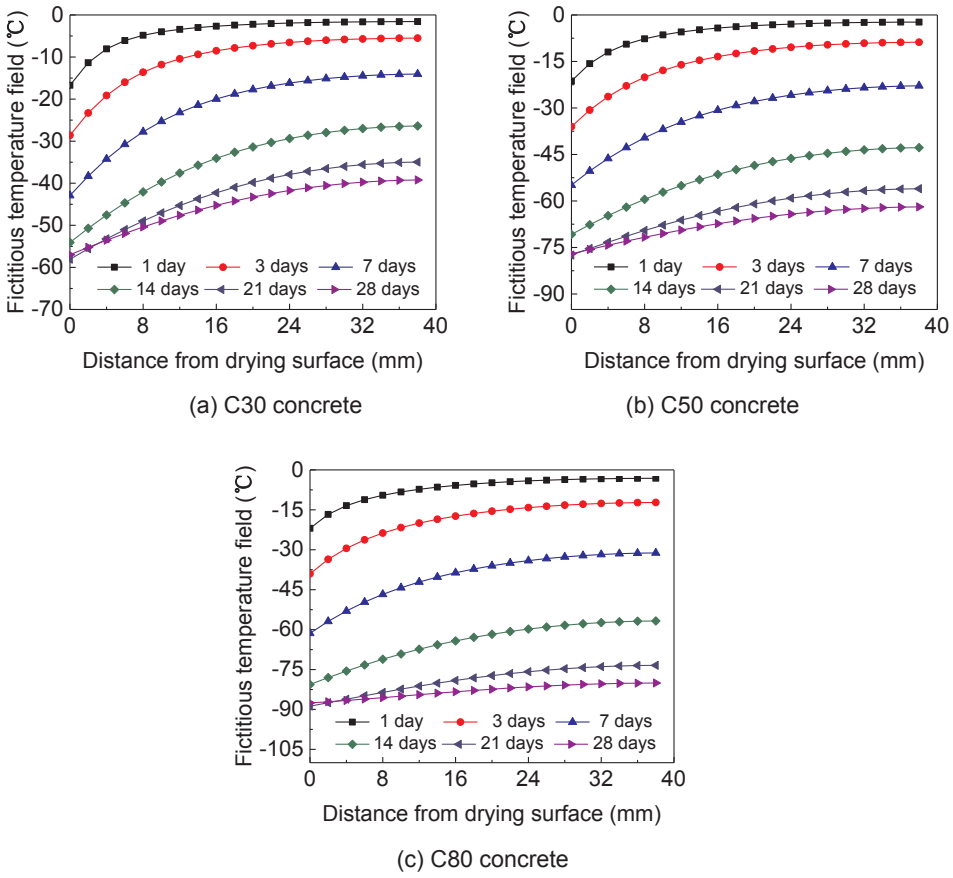

Fig. 10. Distributions of fictitious temperature fields in concretes.

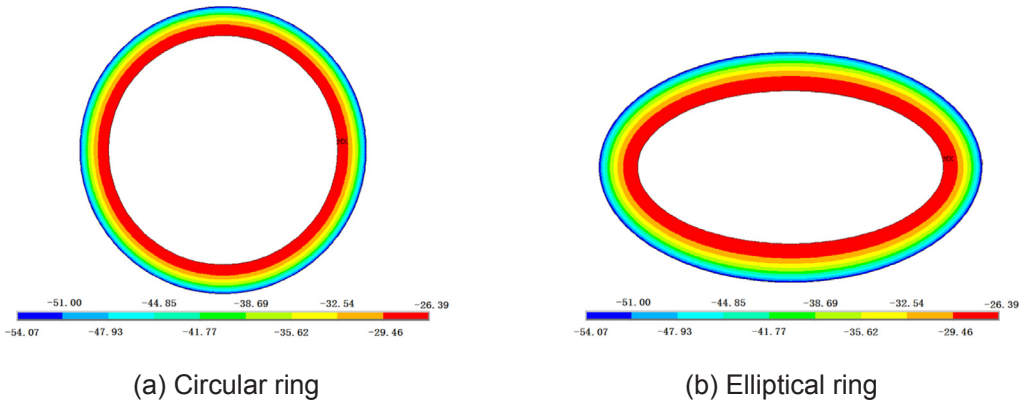

Fig. 11. Fictitious temperature fields of circular and elliptical rings at 14 days for grade C30 concrete.

point in the bilinear σ-w relationship, respectively. The σ-w relationship can be determined by giving fracture energy G_f and tensile strength f_t of concrete, which can be derived from the fitted curves in Fig. 1.

In the fracture analysis, a singular element was used to calculate SIF at the crack tip. Because high-stress gradients exist in the region around crack tip, special attention should be paid in that region. Therefore, a circle was set at the tip of the crack, in which the crack tip is the centre of the circle and the radius of the circle is 2 mm. The first row of elements around the crack tip have a radius of 1/2 mm, and their mid-side nodes were placed at the quarter points, i.e. had a radius of 1/8 mm. Before and after applying the cohesive force on the fictitious crack, the SIFs caused by shrinkage effect (K_I^S) and the combined effect of shrinkage and cohesive force (K_I^S-K_I^σ) were calculated by displacement extrapolation method. In addition, a concrete crack propagation criterion [38,39] based on the initial fracture toughness of concrete was utilized to determine the crack propagation of a concrete ring under restrained

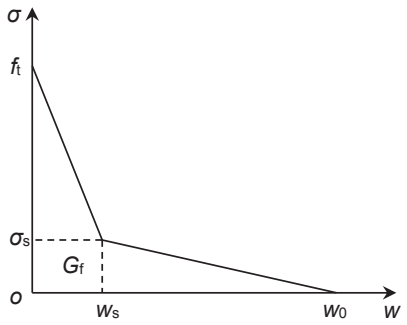

Fig. 12. Bilinear σ-w softening curve for concrete.

shrinkage condition. This criterion can be described as follows: a crack begins to propagate when the difference between the stress intensity factor (SIF) caused by the shrinkage effect K_I^S, and by the cohesive stress, K_I^σ, exceeds the initial fracture toughness of concrete, K_{IC}^{ini}. The criterion can be described as follows:

$$K_I^S - K_I^\sigma < K_{IC}^{ini}, \text{ crack does not propagate} \tag{8}$$

$$K_I^S - K_I^\sigma = K_{IC}^{ini}, \text{ crack is in the critical state} \tag{9}$$

$$K_I^S - K_I^\sigma > K_{IC}^{ini}, \text{ crack propagates} \tag{10}$$

The flow chart of numerical simulation is illustrated in Fig. 13, and the iteration process can be summarized as follows:

1. Input data, the initial crack length $a(1) = 2$ mm.
2. Establish a numerical model for a restrained concrete ring with the crack length $a(i) = a(i - 1) + \Delta a$ ($i = 2, 3\ldots$). Here, Δa is a specified increment of crack length in the numerical analysis, which was chosen as 2 mm in this study. i represents the crack propagation step during the iteration process.
3. Apply the fictitious temperature field of the jth day $T(j)$ ($j = 1, 2\ldots$) and calculate the fictitious temperature distribution caused by $T(j)$ in the thermal analysis. Here, j represents the age during the iteration process corresponding to the crack length.
4. Calculate the crack opening displacement and cohesive stress $\sigma_{i,j}$ using Eqs. (5)–(7). Then, apply the $\sigma_{i,j}$ on the opening crack and calculate $K_I^S - K_I^\sigma$. Increase j and re-calculate $K_I^S - K_I^\sigma$ until the crack propagation criterion (i.e. Eq. (10)) is satisfied.
5. Repeat steps 2–4 for the next crack propagation. The iterative process terminates when the crack length $a(i)$ becomes greater than 37.5 mm or the age j reaches 28 days.

Therefore, the crack initiation time and crack propagation process can be obtained by repeating the above exercise. Taking grade C30 concrete rings as examples, Fig. 14 illustrates the deformation contours of the restrained concrete circular and elliptical rings when the initial crack propagates to 20 mm long at the crack initiation age.

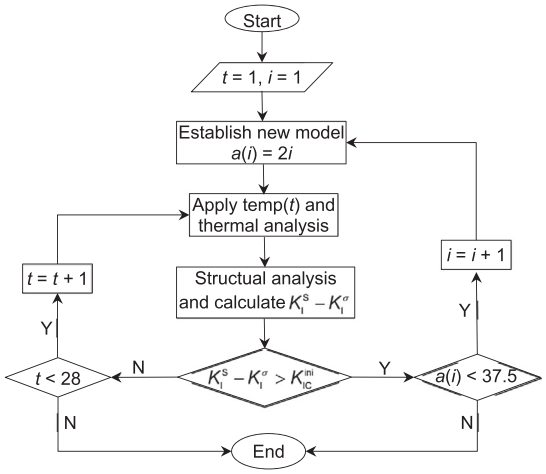

Fig. 13. Flowchart of numerical simulations.

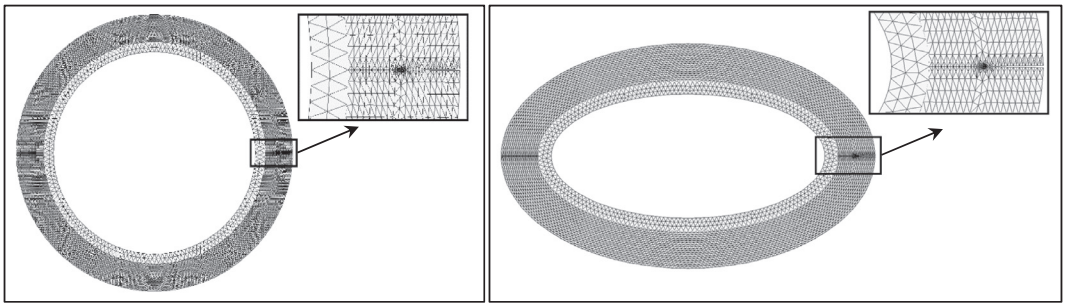

Fig. 14. Deformations of the restrained circular and elliptical concrete rings.

4. Results and discussion

4.1. Crack initiation and propagation process

In fracture analysis, the initial crack should be set on the position where the maximum tensile stress occurs in a concrete ring. For the circular rings, the values of tensile stress along their circumference are the same, while for the elliptical rings, the stress values will reach their maximum at the vertex along the major axis [25,26]. Fig. 15 illustrates the distributions of the age-dependent tensile stress in circular/elliptical concrete rings along their radial direction. The random and major radical cross-sections were selected for the circular and elliptical concrete rings, respectively. It should be noted that the calculated tensile stresses in Fig. 15 are unreasonably high due to the effect of the non-uniform shrinkage along the radial direction of a concrete ring. This can be considered as the initiation of the micro-cracks when the maximum tensile stress is much higher than the concrete tensile strength, rather than the initiation of the macro-cracks. In fact, the tensile stress distributions calculated by elastic analyses were used to determine the position of the maximum tensile stress, i.e. the potential cracking position. And then, the age of the initiation of macro-crack was determined using the fracture mechanics-based method mentioned in this study. Based on the elastic analysis of the tensile stress distribution, the position where the maximum tensile stress occurs, and the shrinkage crack initials can be determined. For the circular rings, the tensile stress at the inner surface is always less than its counterpart at the outer surface from 1 to 28 days (except for the circular ring made of grade C80 concrete at 28 days). This means that the restrained shrinkage cracks in circular rings will initiate at their outer surface and propagate towards their inner surface. However, the scenario is different for the elliptical rings since he tensile stress at the inner surface is greater than that at the outer surface at later ages for the concretes with three strength grades. With the increase of concrete strength, the difference between the outer and inner surfaces of a concrete ring becomes more significant. According to the results in Fig. 15, for the elliptical rings made of grade C30, C50 and C80 concrete, the critical ages when the tensile stress at the inner surface exceeds that of the outer surface are 23, 16 and 12 days, respectively. Therefore, in the case of an elliptical geometry, a 2 mm-long initial crack was firstly set at the outer surface of the elliptical concrete ring. If the predicted cracking age was less than the corresponding critical age, the shrinkage crack in the concrete ring would initiate at its outer surface. Otherwise, the initial crack should be set at inner surface of the concrete ring in fracture analysis. In addition, according to the comparisons of stress distributions between the circular and elliptical rings, it can be concluded that the elliptical ring can provide higher restraint to the concrete under drying shrinkage and cause higher tensile stress in concrete. Particularly, the maximum tensile stress occurs at the inner surface of the concrete ring, indicating that the fracture of concrete is dominated by the restraint from the inner steel ring.

After determining the position of the initial crack, the crack propagation can be judged by taking a comparison between $K_I^S - K_I^\sigma$ and K_{IC}^{ini}. Fig. 16 illustrates the variations of $K_I^S - K_I^\sigma$ and K_{IC}^{ini} with the increase of age for the concretes with three strength grades. It can be seen that the values of $K_I^S - K_I^\sigma$ and K_{IC}^{ini} increase with the increase of age. However, at the same age, the values of $K_I^S - K_I^\sigma$ in the elliptical rings are greater than the ones in the circular rings. This indicates that, compared with the circular geometry, the elliptical one can provide a much larger restraint for the outer concrete. For the circular rings, the values of $K_I^S - K_I^\sigma$ reach K_{IC}^{ini} at 18, 15 and 10 days for C30, C50 and C80 concretes, respectively. In contrast, for the elliptical ring, the corresponding ages are 14, 12 and 7 days, which are 3–4 days earlier. It should be noted that according to the results presented in Fig. 15, the ages for the initial crack propagation in the elliptical rings are less than the critical ages, i.e. the age when the tensile stress at the inner surface becomes greater than the one at the outer surface. Therefore, for the concretes investigated in this study, the crack will initiate at the outer surfaces of the concrete rings.

Once the initial crack begins to propagate, what is of concern is how the crack propagates throughout the cross-section of a concrete ring. Fig. 17 illustrates the relationship of $K_I^S - K_I^\sigma$ and K_{IC}^{ini} with the crack length corresponding to the age of initial crack propagation. It can be seen that $K_I^S - K_I^\sigma$ keeps increasing with the increase of crack length, indicating that the crack will propagate throughout the whole cross-section of a concrete ring once it initiates. The cracking ages from experiment and numerical simulation are listed in Table 4, which show good agreement, suggesting that the proposed numerical method is appropriate and accurate.

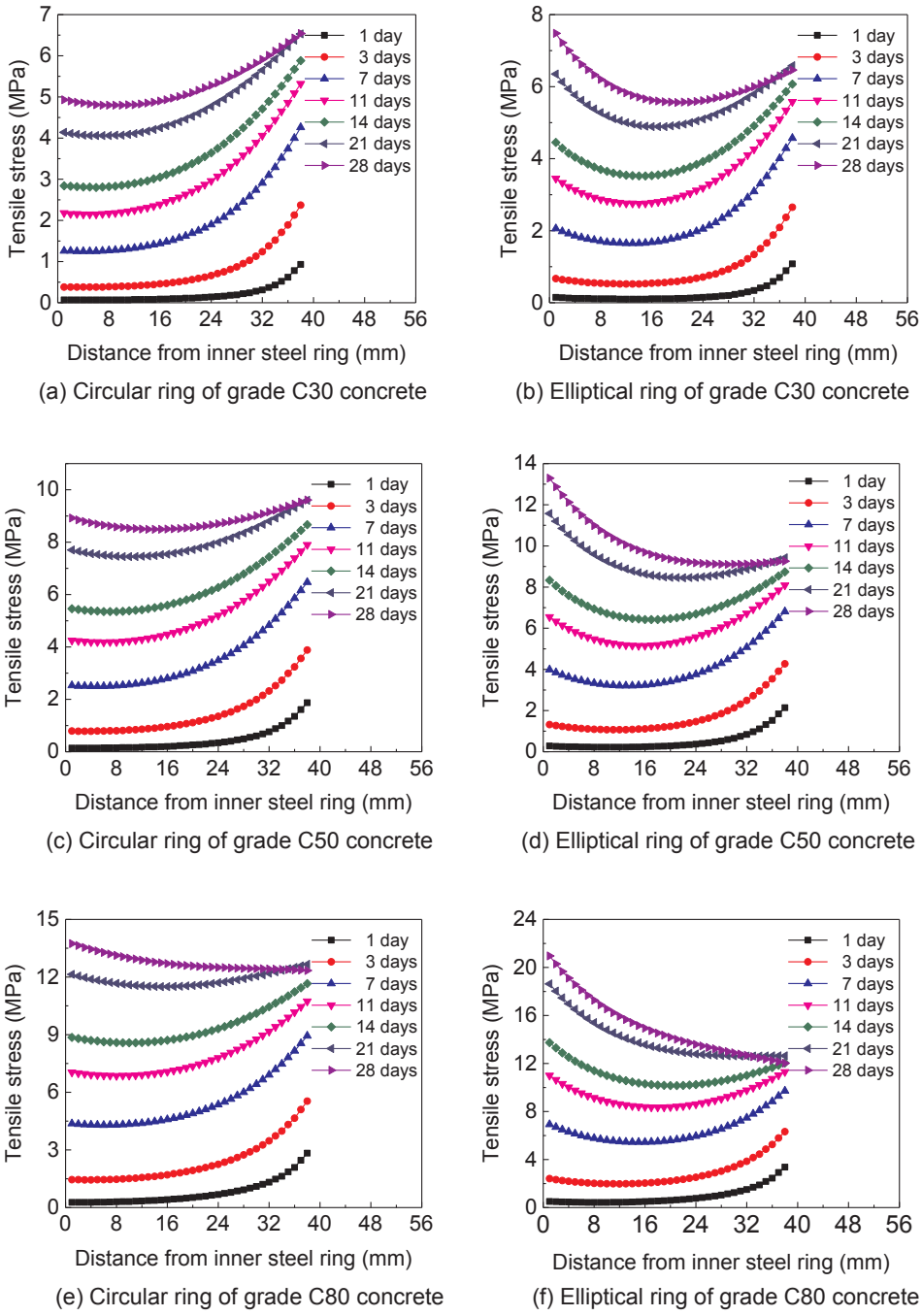

Fig. 15. Stress distributions along the radial direction of the concrete ring for different concrete grades.

4.2. Composition of restraint effect: self-restraint vs. external restraint (i.e. steel ring restraint)

In the ring tests, the restraint effects on a concrete ring consist of two parts, i.e. the self-restraint caused by the non-uniform shrinkage and the external restraint from the steel ring. For a 75 mm-thick ring specimen under outer circumference drying, it has been proven that the crack initiation and propagation is mainly driven by the self-restraint rather than by the external restraint from the steel ring due to the significant non-uniform shrinkage along the radial direction [17]. However, the main purpose of the restrained ring test was to assess the cracking resistance of concrete under external restraint. To reduce the self-restraint caused by non-uniform shrinkage, drying from the top and bottom surfaces was employed by many researchers in the restrained ring tests [13,18–20]. In addition, the thinner concrete ring, i.e. with the ring wall thickness of 37.5 mm, was adopted. However, in this case,

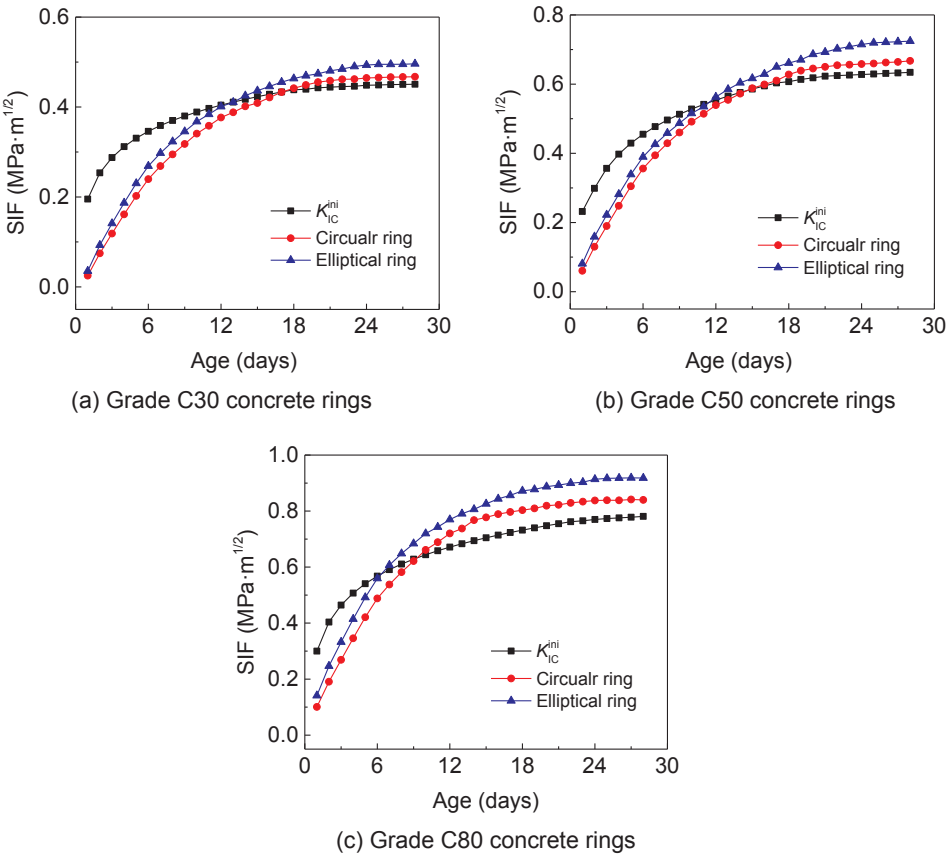

Fig. 16. Variations of $K_I^S - K_I^\sigma$ and K_{IC}^{ini} at different ages.

the effect of the moisture gradient is still significant for the ring specimen due to the highly nonlinear moisture distribution in concrete. In addition, different moisture distributions exist in the concrete with various strength grades, resulting in the changes of the composition of restraint effect in the ring tests. Therefore, it is significant to quantify the effect of self-restraint and external restraint on the crack propagation process in the restrained concrete ring with various strength grades.

It has been verified that the crack will propagate throughout the cross-section from outer to inner surfaces after its initiation. To calculate the SIFs under self-restraint during the crack propagation process, the finite element model of the concrete ring without inner steel ring was established. By applying the fictitious temperature field at the age of crack initiation, the SIFs only caused by self-restraint, $K_{I\,self}^S$, can be calculated by thermal and structural analyses. Meanwhile, the SIFs caused by steel ring restraint, $K_{I\,steel}^S$, can be obtained from the difference between the total restraint effects, K_I^S,and self-restraint effect, $K_{I\,self}^S$, i.e. $K_{I\,steel}^S = K_I^S - K_{I\,self}^S$. Fig. 18 illustrates the variations of the stress intensity factors (SIFs) caused by self-restraint and external restraint with respect to different crack lengths at the cracking age. It can be seen that, for all the concrete rings examined in this study, the crack initiations are caused by a combination of self-restraint and external restraint from the central steel ring. Meanwhile, the proportion of external restraint is greater than self-restraint. As crack propagates, the effect of external restraint increases sharply, while the effect of self-restraint increases slowly, and even decreases when the crack is close to the inner surface of the concrete ring.

To quantify the proportion of the restraint effect, Fig. 19 illustrates the SIF ratios of $K_{I\,steel}^S$ to K_I^S for the concretes with three strength grades. Here, $K_{I\,steel}^S$ is the SIF caused by external restraint (i.e. by the central steel ring), and K_I^S is the SIF caused by the total restraint including self-restraint and external restraint. It can be seen that, for all the concrete rings investigated in this study, the ratios of $K_{I\,steel}^S$ to K_I^S are all greater than 0.6 when the initial cracks begin to propagate and the ratios increase significantly during the crack propagation processes. The results indicate that, in the case of 37.5 mm-thick concrete ring specimens, the steel ring restraint plays the leading role for driving the crack initiation and propagation, which is different from the case of 75 mm-thick concrete rings. Meanwhile, for both circular and elliptical rings, the ratios of $K_{I\,steel}^S$ to K_I^S increase with the increase of the concrete strength grades. This is because the moisture distribution along the radial direction becomes insignificant with the increase of concrete strength so that the restraint caused by the non-uniform shrinkage decreases. In addition, the ratios of $K_{I\,steel}^S$ to K_I^S for elliptical rings are greater than those for the circular ones, resulted from the contribution of the elliptical geometry.

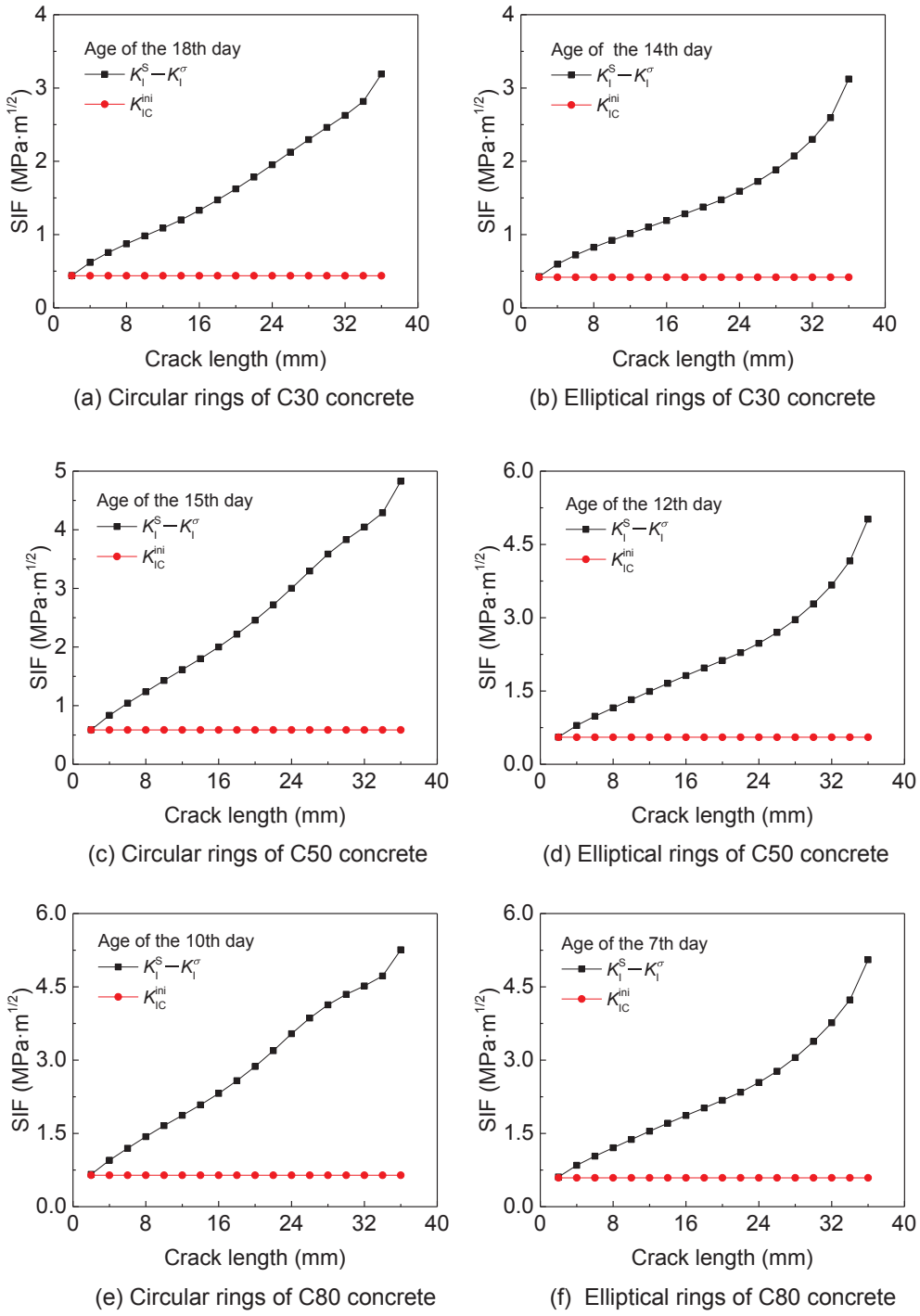

Fig. 17. Variations of $K_I^S - K_I^\sigma$ and K_{IC}^{ini} with crack lengths.

4.3. Assumption of uniform shrinkage

It has been verified that the moisture gradient (consequently caused non-uniform shrinkage) along the radial direction of a concrete ring should be considered when analyzing the fracture mechanism of a restrained shrinkage concrete ring under outer circumference drying. However, the moisture gradient becomes more insignificant with the increase of concrete strength. In this case, for the purpose of computational simplification, the uniform shrinkage assumption along the radial direction was adopted in the crack propagation analysis [21–27]. However, it is not clear whether the assumption is appropriate for the investigation of fracture

Table 4
Comparison of cracking ages (in days) from experiment and numerical simulation.

Cracking ages	C30 concrete		C50 concrete		C80 concrete	
	Exp.	Num.	Exp.	Num.	Exp.	Num.
Circular	21	18	16	15	11	10
Elliptical	17	14	11	12	9	7

mechanism in the ring test. Meanwhile, there are no studies on the comparison of the fracture behaviour in the ring specimens when the uniform and non-uniform shrinkage assumptions are adopted in literature. Therefore, both the uniform and non-uniform shrinkage assumptions were employed in this study to compare the shrinkage cracking of the restrained concrete rings with three distinguished strength grades.

Under the uniform shrinkage assumption, the fictitious temperature field used to simulate the concrete shrinkage can be obtained by dividing the free shrinkage strain of the prismatic specimens by the coefficient of thermal expansion of concrete (in this case the value 10×10^{-6}/℃ is taken). Fig. 20 illustrates the fictitious temperature drops for ring specimens with the three strength grades from 1 to 28 days.

According to previous studies [25,27], for a ring specimen subject to uniform shrinkage, the first crack initiates at the inner surface of a concrete ring and propagates towards its outer surface. Therefore, a 2 mm-long initial crack was set at the inner surface of the cross-section of a concrete ring, randomly along the circumference of the circular ring and along the major axis of the elliptical ring. Based on the thermal and structural analyses, the values of $K_{\mathrm{I}}^{\mathrm{S}} - K_{\mathrm{I}}^{\sigma}$ and $K_{\mathrm{IC}}^{\mathrm{ini}}$ were derived with the increase of age for the concrete circular/elliptical rings with three strength grades, with the results presented in Fig. 21. It can be seen that the values of $K_{\mathrm{I}}^{\mathrm{S}} - K_{\mathrm{I}}^{\sigma}$ and $K_{\mathrm{IC}}^{\mathrm{ini}}$ increase with the increase of age. However, at the same age, the values of $K_{\mathrm{I}}^{\mathrm{S}} - K_{\mathrm{I}}^{\sigma}$ in the elliptical rings are greater than those in the circular rings. In some cases, e.g. the circular rings of C30 and C50 concrete, the values of $K_{\mathrm{I}}^{\mathrm{S}} - K_{\mathrm{I}}^{\sigma}$ do not exceed the $K_{\mathrm{IC}}^{\mathrm{ini}}$ until the age of 28 days, which means that shrinkage cracking does not occur. The cracking ages for all ring specimens under uniform and non-uniform shrinkage assumptions are listed in Table 5. Num1. and Num2. denote the predicted cracking ages under the non-uniform and uniform shrinkage assumptions, respectively. In addition, the relative errors of cracking ages between the experiment and numerical simulations are listed in the brackets of Table 5.

It can be seen that the cracking ages calculated under the two assumptions exhibit great differences. Under uniform shrinkage assumption, the predicted cracking ages are significantly larger than the experimental results ($\geq$33.3%). In contrast, based on the non-uniform shrinkage assumption, the relative errors of cracking ages between the experimental and numerical range from 9.1% to 22.2%. As aforementioned, in the ring test, the restraint driving the crack initiation and propagation includes that from the inner steel (i.e. external restraint) as well as that due to the non-uniform shrinkage of the cross-section (i.e. internal restraint) of a concrete ring. According to the results shown in Fig. 19, the ratios of steel ring restraint to total restraint corresponding to crack initiation, are 60.5%, 63.5%, 65.6% with respect to C30, C50, C80 concrete circular rings, respectively. Meanwhile, in the case of C30, C50, C80 concrete elliptical rings, the ratios are 65.6%, 67.8%, 70.6%, respectively. Under the uniform shrinkage assumption, the restraint effect to drive the crack initiation and propagation will be provided only from steel ring restraint in numerical analyses and the self-restraint caused by non-uniform shrinkage was totally neglected, resulting in underestimation of the driving force. Therefore, there are obvious differences of the cracking ages and restraint effects between the experiment and numerical simulation under uniform shrinkage assumption, suggesting that uniform shrinkage assumption is not appropriate.

As a summary, there are two significant differences on the predicted results using the uniform and non-uniform shrinkage assumptions, respectively, which are the crack initiation position and the component of the restraint. Under the uniform shrinkage assumption, the crack will initiate at the inner surface of the concrete ring and propagate towards its outer surface. The external restraint from the inner steel ring provides the only driving force to trigger the cracking in the concrete ring. In contrast, under the non-uniform shrinkage assumption, the crack will initiate at the outer surface of the concrete ring and propagates towards its inner surface. Both the external restraint from the inner steel ring and the internal restraint due to non-uniform shrinkage of concrete contribute to the cracking initiation and propagation in the concrete ring. Therefore, from the point of view of having a deeper understanding of the fracture mechanism of the restraint shrinkage ring tests, it is more appropriate to consider the effect of the non-uniform shrinkage caused by the moisture gradient in concrete.

5. Conclusions

To investigate the effect of the moisture gradient of concrete on the fracture process in the restrained concrete ring, three series of circular and elliptical concrete rings with three distinguished strength grades of C30, C50 and C80 were tested under restrained shrinkage until cracking occurred. By introducing an integrative model to calculate the moisture distribution, the fictitious temperature field was derived to simulate the shrinkage effect of concrete. A numerical approach based on fracture mechanics was developed to analyze the crack initiation and propagation process. Based on the experimental and numerical studies, the following conclusions can be drawn:

(1) A fracture mechanics-based numerical method was employed in this study to simulate the whole fracture process shrinkage in restrained shrinkage ring tests. The nonlinear property of concrete was taken into consideration and the fracture process,

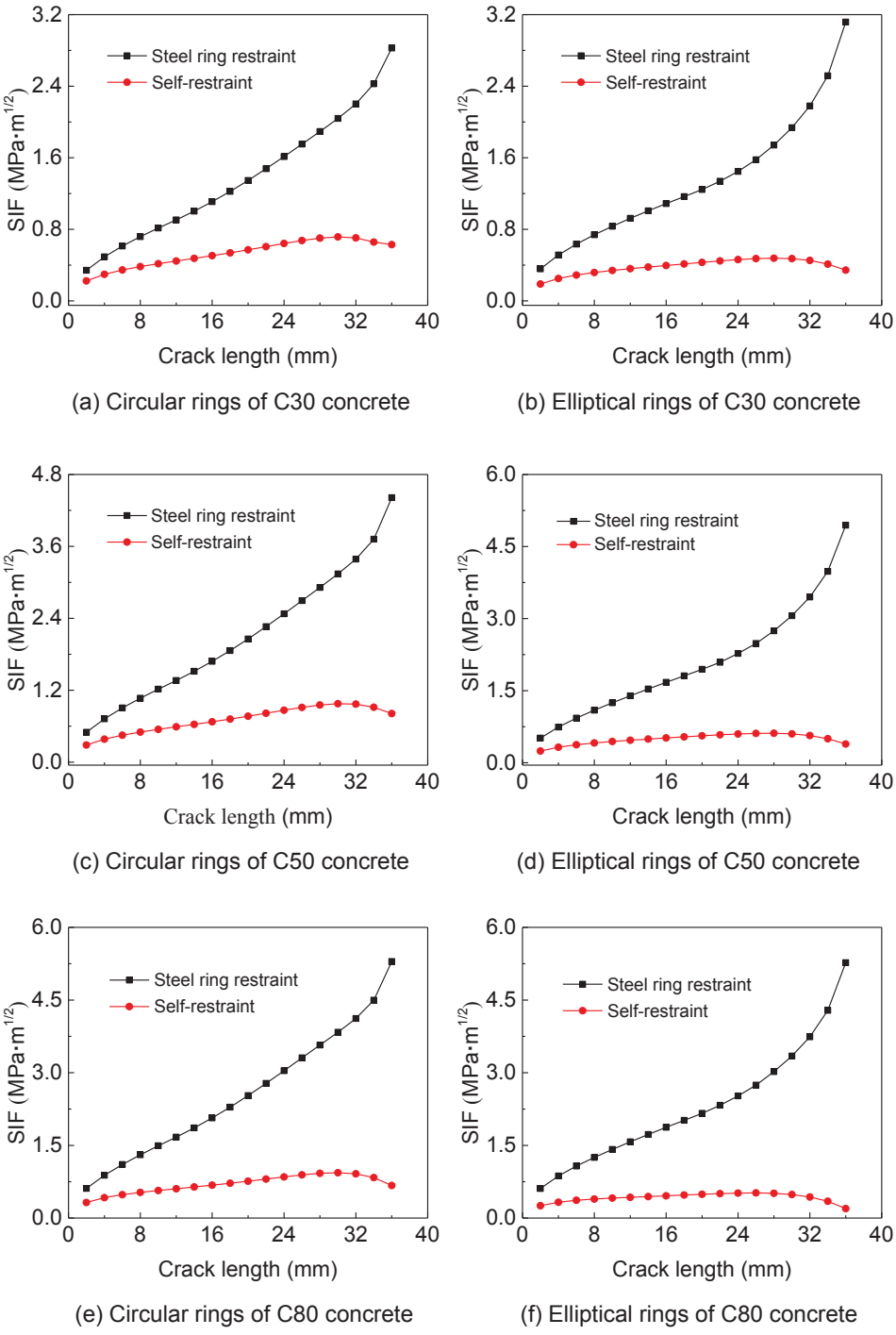

Fig. 18. SIFs caused by self-restraint and external restraint during crack propagation.

including crack initiation and propagation was analysed. The numerical method was verified by taking a comparison of the cracking ages between the numerical and experimental results, which shows a reasonably good agreement.

(2) Based on the experimental and numerical analyses, it can be found that the moisture gradient-induced non-uniform shrinkage along the radial direction has significant effects on the cracking potential of 37.5 mm-thick ring specimens. As for all circular and elliptical concrete rings with strength grades of C30, C50 and C80, the cracks initiate at the outer surfaces of the concrete rings and propagate towards their inner surfaces. In addition, the crack would propagate throughout the whole cross-section of the concrete ring once it initiates.

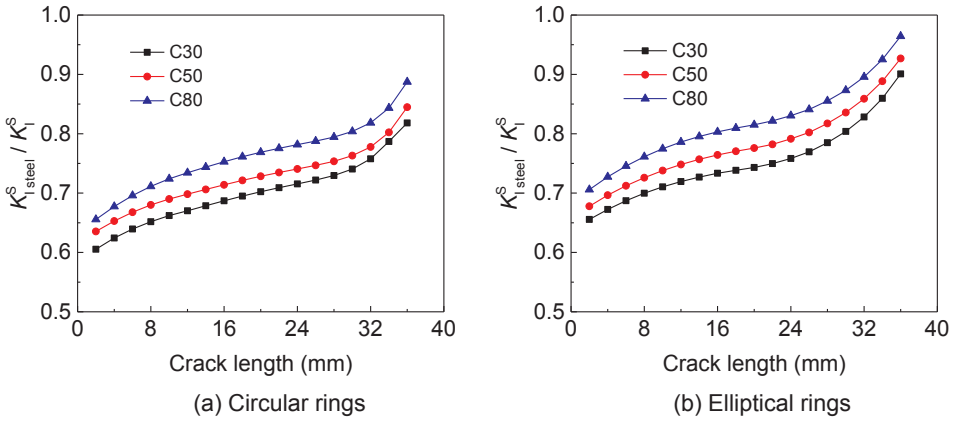

Fig. 19. Ratios of $K^S_{I\,steel}$ to K^S_I in crack propagation process.

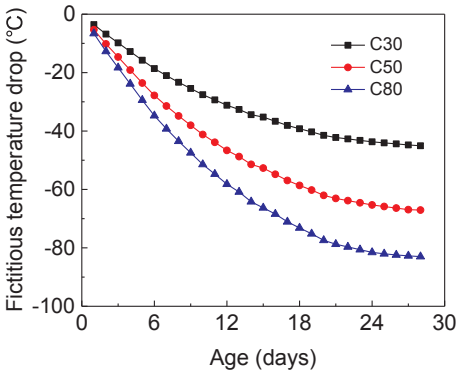

Fig. 20. Fictitious temperature field under the assumption of uniform shrinkage.

(3) With the increase of concrete strength, the restrained concrete ring cracked earlier, indicating that the high strength concrete is more sensitive to shrinkage cracking in the ring test. In addition, numerical analyses revealed that the elliptical ring can provide more restraint to the shrinkage of the concrete ring and accordingly increase the tensile stress level, resulting in earlier cracking in elliptical concrete rings. However, the increasing restraint effects are more obvious at the inner surface of the concrete ring, which may cause the crack initiate on the inner surface of the ring.

(4) Under outer circumference drying, the driving force for crack propagation was provided by both the self-restraint caused by non-uniform shrinkage of concrete and the external restraint caused by the inner steel ring with the external restraint playing the leading role (greater than 60%) to drive the fracture process. With the increase of concrete strength, the proportion of the external restraint in the total restraint increases because of the insignificant moisture distribution in the concrete ring.

(5) If adopting the uniform shrinkage assumption to investigate the cracking potential in restrained shrinkage ring test, the self-restraint effect could not be taken into account, so that the steel ring restraint would be overestimated accordingly. In addition, the crack will initiate at the inner surface of the concrete ring and propagate to its outer surface, which contradicts the findings by considering the realistic non-uniform shrinkage in concrete. Therefore, from the point of the view of having deeper understanding on the fracture mechanism of the restraint shrinkage ring test, the non-uniform shrinkage in a restrained concrete ring should not be simplified as the uniform one in numerical analyses.

Acknowledgements

The authors gratefully acknowledge the financial support of the National Natural Science Foundation of China under the grants of NSFC 51478083 and NSFC 51421064, the Engineering and Physical Sciences Research Council under the grant of EP/I031952/1, Fundamental Research Funds for the Central Universities of China under the grants of DUT17LK06 and the National Basic Research Program of China (the 973 Program) under the grant of 2015CB057703.

Appendix A. Supplementary material

Supplementary data to this article can be found online at https://doi.org/10.1016/j.engfracmech.2019.01.011.

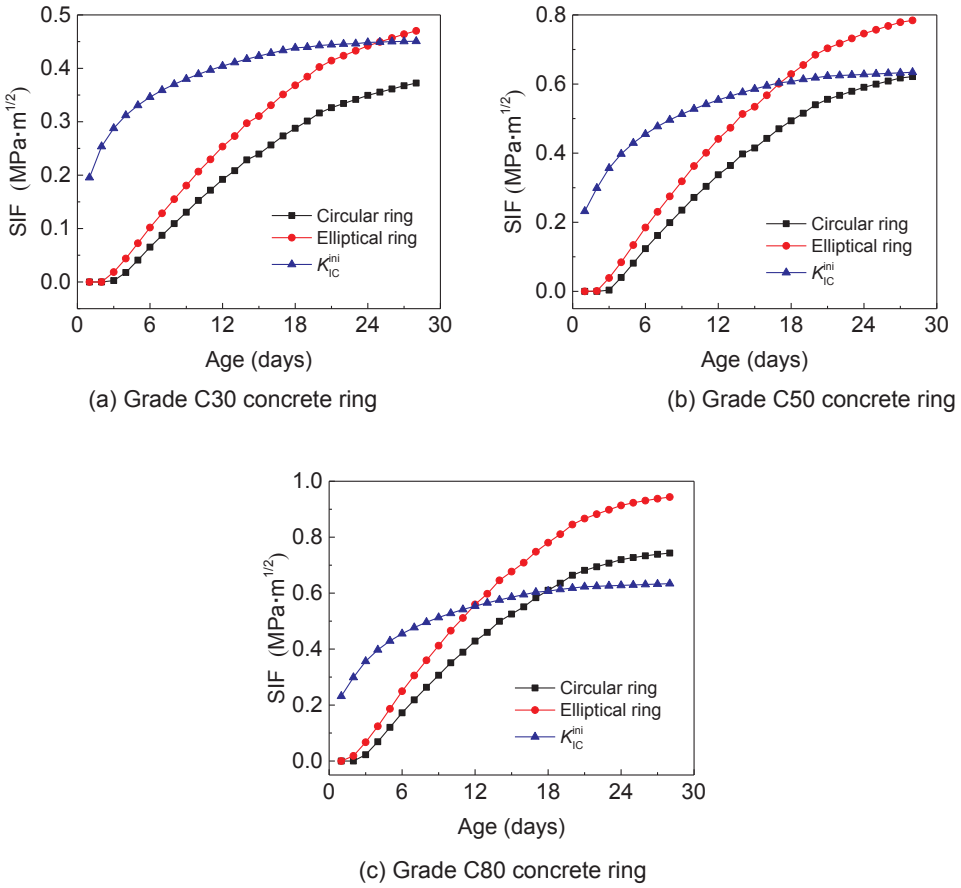

Fig. 21. Values of $K_I^S - K_I^\sigma$ and K_{IC}^{ini} for three concrete grades under uniform shrinkage assumption.

Table 5
Cracking ages (days) and relatively errors under uniform and non-uniform shrinkage assumptions[1].

Cracking ages (Relative errors)	C30 concrete		C50 concrete		C80 concrete	
	Num1.	Num2.	Num1.	Num2.	Num1.	Num2.
Circular	18 (14.3%)	–	15 (6.3%)	–	10 (9.1%)	18 (63.6%)
Elliptical	14 (21.4%)	25 (47.1%)	12 (9.1%)	19 (72.7%)	7 (22.2%)	12 (33.3%)

[1] "–" means no simulated crack initiation up to 28 days.

References

[1] Wang K, Jansen DC, Shah SP, et al. Permeability study of cracked concrete. Cem Concr Res 1997;27(3):381–93.
[2] Banthia N, Gupta R. Influence of polypropylene fiber geometry on plastic shrinkage cracking in concrete. Cem Concr Res 2006;36(7):1263–7.
[3] Soliman AM, Nehdi ML. Effects of shrinkage reducing admixture and wollastonite microfiber on early-age behavior of ultra-high performance concrete. Cem Concr Compos 2014;46(4):81–9.
[4] Cusson D, Hoogeveen T. Internal curing of high-performance concrete with pre-soaked fine lightweight aggregate for prevention of autogenous shrinkage cracking. Cem Concr Res 2008;38(6):757–65.
[5] Bentur A, Kovler K. Evaluation of early age cracking characteristics in cementitious systems. Mater Struct 2003;36(3):183–90.
[6] Carlson RW, Reading TJ. Model of studying shrinkage cracking in concrete building walls. ACI Struct J 1988;85(4):395–404.
[7] Weiss WJ, Yang W, Shah SP. Influence of specimen size/geometry on shrinkage cracking of rings. ASCE J Eng Mech 2000;126(1):93–101.
[8] Moon JH, Rajabipour F, Pease B, et al. Quantifying the influence of specimen geometry on the results of the restrained ring test. J ASTM Int 2006;3(8):1–14.
[9] Zhen H, Zhou XM, Li ZJ. New experimental method for studying early-age cracking of cement-cased materials. ACI Mater J 2004;101(1):50–6.
[10] Dong W, Zhou XM, Wu ZM, et al. Quantifying the influence of elliptical ring geometry on the degree of restraint in a ring test. Comput Struct 2018;207(9):111–20.
[11] Hossain AB, Weiss WJ. The role of specimen geometry and boundary conditions on stress development and cracking in the restrained ring test. Cem Concr Res 2006;36(1):189–99.
[12] Dong W, Yuan WY, Zhou XM, et al. The fracture mechanism of circular/elliptical concrete rings under restrained shrinkage and drying from top and bottom surfaces. Eng Fract Mech 2017;189:148–63.
[13] Weiss WJ, Shah SP. Restrained shrinkage cracking: the role of shrinkage reducing admixtures and specimen geometry. Mater Struct 2002;35(2):85–91.

[14] Moon JH, Weiss WJ. Estimating residual stress in the restrained ring test under circumferential drying. Cem Concr Compos 2006;28(5):486–96.
[15] Seung HK, Shah SP. Prediction of early-age cracking of fiber-reinforced concrete due to restrained shrinkage. ACI Mater J 2008;105(4):381–9.
[16] Shah SP, Grzybowski M. Model to predict cracking in fibre reinforced concrete due to restrained shrinkage. Mag Concrete Res 1989;41(148):125–35.
[17] Dong W, Zhou XM, Wu ZM, et al. Effects of specimen size on assessment of shrinkage cracking of concrete via elliptical rings: thin vs. thick. Comput Struct 2016;174(SI):66–78.
[18] Hossain AB, Weiss WJ. Assessing residual stress development and stress relaxation in restrained concrete ring specimens. Cem Concr Compos 2004;26(5):531–40.
[19] Turcry P, Loukili A, Haidar K, et al. Cracking tendency of self-compacting concrete subjected to restrained shrinkage: experimental study and modeling. ASCE J Mater Civil Eng 2006;18(1):46–54.
[20] Shah HR, Weiss WJ. Quantifying shrinkage cracking in fiber reinforced concrete using the ring test. Mater Struct 2006;39(9):887.
[21] Grzybowski M. Shrinkage cracking of fiber reinforced concrete. ACI Mater J 1990;87(2):138–48.
[22] Shah SP, Ouyang CS, Marikunte S, et al. A method to predict shrinkage cracking of concrete. ACI Mater J 1998;95(4):339–46.
[23] Miltenberger MA, Attiogbe EK, See HT. Shrinkage cracking characteristics of concrete using ring specimens. ACI Mater J 2003;100(3):239–45.
[24] Dean SW, Raoufi K, Bernard ES, et al. Shrinkage cracking behavior of fiber reinforced concrete: as assessed using the restrained ring test. J ASTM Int 2010;7(7):1–15.
[25] Dong W, Zhou XM, Wu ZM. A fracture mechanics-based method for prediction of cracking of circular and elliptical concrete rings under restrained shrinkage. Eng Fract Mech 2014;131:687–701.
[26] Zhou XM, Dong W, Oladiran O. Experimental and numerical assessment of restrained shrinkage cracking of concrete using elliptical ring specimens. ASCE J Mater Civil Eng 2014;26(11):04014087.
[27] Dong W, Zhou XM, Wu ZM, et al. Investigating crack initiation and propagation of concrete in restrained shrinkage circular/elliptical ring test. Mater Struct 2017;50(1):1–13.
[28] Bažant ZP, Najjar LJ. Nonlinear water diffusion in nonsaturated concrete. Mater Struct 1972;5(1):3–20.
[29] Xi Y, Bažant ZP, Jennings HM. Moisture diffusion in cementitious materials adsorption isotherms. Adv Cem Based Mater 1994;1(6):248–57.
[30] Parrott LJ. Moisture profiles in drying concrete. Adv Cem Res 1988;1(3):164–70.
[31] Mcdonald DB, Roper H, Parrott LJ. Discussion: factors influencing relative humidity in concrete. Mag Concrete Res 1991;43(157):305–7.
[32] Zhang J, Hou DW, Gao Y, et al. Determination of moisture diffusion coefficient of concrete at early-age from interior humidity measurements. Dry Technol 2011;6(29):689–96.
[33] Zhang J, Qi K, Huang Y. Calculation of moisture distribution in early-age concrete. ASCE J Eng Mech 2009;135(8):871–80.
[34] Zhang J, Huang Y, Qi K, et al. Interior relative humidity of normal- and high-strength concrete at early age. ASCE J Mater Civil Eng 2012;6(24):615–23.
[35] Zhang J, Yuan G, Han YD. Evaluation of shrinkage induced cracking in early age concrete: from ring test to circular column. Int J Damage Mech 2017;26(5):771–97.
[36] Zhang J, Hou DW, Chen H. Experimental and theoretical studies on autogenous shrinkage of concrete at early ages. ASCE J Mater Civil Eng 2011;23(3):312–20.
[37] Hillerborg A, Modéer M, Petersson PE. Analysis of crack formation and crack growth in concrete by means of fracture mechanics and finite elements. Cem Concr Res 1976;6(6):773–81.
[38] Dong W, Wu ZM, Zhou XM. Calculating crack extension resistance of concrete based on a new crack propagation criterion. Constr Build Mater 2013;38(2):879–89.
[39] Dong W, Zhou XM, Wu ZM. On fracture process zone and crack extension resistance of concrete based on initial fracture toughness. Constr Build Mater 2013;49(6):352–63.
[40] RILEM Committee FMC50. Determination of the fracture energy of mortar and concrete by means of three-point bend tests on notched beams. Mater Struct 1985;18:285–90.
[41] Xu SL, Reinhardt HW. Determination of double-K criterion for crack propagation in quasi-brittle fracture, Part II: Analytical evaluating and practical measuring methods for three-point bending notched beams. Int J Fracture 1999;98(2):151–77.
[42] Kovler K, Bentur A. Cracking sensitivity of normal- and high-strength concretes. ACI Mater J 2009;106(6):537–42.
[43] Zhang J, Hou HD, Wei S. Experimental study on the relationship between shrinkage and interior humidity of concrete at early age. Mag Concrete Res 2010;62(3):191–9.
[44] Kovler K. Drying creep of concrete in terms of the age-adjusted effective modulus method. Mag Concrete Res 1997;49(181):345–51.
[45] Oh BH, Cha SW. Nonlinear analysis of temperature and moisture distributions in early-age concrete structures based on degree of hydration. ACI Mater J 2003;100(5):361–70.
[46] Ouyang C, Shah SP. Geometry-dependent R-curve for quasi-brittle materials. J Am Ceram Soc 2010;74(11):2831–6.
[47] Petersson PE. Crack growth and development of fracture zones in plain concrete and similar materials. Report TVBM-1006. Sweden: Division of Building Materials, Lund Institute of Technology; 1981.